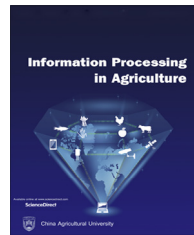




Available at www.sciencedirect.com

INFORMATION PROCESSING IN AGRICULTURE 4 (2017) 64–77

journal homepage: www.elsevier.com/locate/inpa



Finite element analysis of the dynamic behavior of pear under impact loading



Alireza Salarikia, Seyed-Hassan Miraei Ashtiani*, Mahmood Reza Golzarian,
Hamid Mohammadinezhad

Department of Biosystems Engineering, Faculty of Agriculture, Ferdowsi University of Mashhad, Mashhad, Iran

ARTICLE INFO

Article history:

Received 27 June 2016

Received in revised form

4 October 2016

Accepted 28 December 2016

Available online 3 January 2017

Keywords:

Bruising

Dropping impact

FEM

Contact force

Stress-strain distribution

Reverse engineering

ABSTRACT

Pear fruit is susceptible to bruising from mechanical impact during field harvesting operations and at all stages of postharvest handling. The postharvest shelf life of bruised fruits were shorter, and they softened rapidly under cold storage compared with non-bruised samples. Developing strategies for reducing bruising during the supply chain requires an understanding of fruit dynamic behavior to different enforced loadings. Finite Element Method (FEM) is among the best techniques, in terms of accuracy and cost-efficiency, for studying the factors effective in impact-induced bruising. In this research, the drop test of pear sample was simulated using FEM. The simulation was conducted on a 3D solid model of the pear that was created by using non-contact optical scanning technology. This computer-based study aimed to assess the stress and strain distribution patterns within pear generated by collision of the fruit with a flat surface made of different materials. The contact force between two colliding surfaces is also investigated. The simulations were conducted at two different drop orientations and four different impact surfaces. Results showed that, in both drop orientations, the largest and smallest stresses, strains and contact forces were developed in collision with the steel and rubber surfaces, respectively. In general, these parameters were smaller when fruit collided with the surfaces along its horizontal axis than when collided along its vertical axis. Finally, analyses of stress and strain magnitudes showed that simulation stress and strain values were compatible with experiments data.

© 2017 China Agricultural University. Publishing services by Elsevier B.V. This is an open access article under the CC BY-NC-ND license (<http://creativecommons.org/licenses/by-nc-nd/4.0/>).

1. Introduction

For modern human, fruits and vegetables are an inseparable part of a healthy diet, expecting a good quality for them. Tex-

ture is a qualitative property in these products that affects consumer acceptance, shelf life, resistance to diseases and handling [1]. It is essential to have knowledge about the textural properties of horticultural products in order to design and develop farm machinery [2]. With no database available on the basic and mechanical characteristics of agricultural products, engineers should rely on experimental methods to design handling and processing machinery, which that is inefficient in terms of both time and costs [3]. Therefore, there have been efforts to evaluate the effect of impact and quasi-

* Corresponding author at: Department of Biosystems Engineering, Faculty of Agriculture, Ferdowsi University of Mashhad, P.O. Box 9177948978, Mashhad, Iran.

E-mail address: Miraei_sh@yahoo.com (S.-H. Miraei Ashtiani).
Peer review under responsibility of China Agricultural University.

<http://dx.doi.org/10.1016/j.inpa.2016.12.003>

2214-3173 © 2017 China Agricultural University. Publishing services by Elsevier B.V.

This is an open access article under the CC BY-NC-ND license (<http://creativecommons.org/licenses/by-nc-nd/4.0/>).

static loading during harvest and postharvest stages on the mechanical damage to fruits, vegetables and biological matters [4,5]. It is obvious that static and dynamic forces act on horticultural products from origin to end user, as they are exposed to multiple processes [6]. Bruising is the most common symptom for mechanical damage [7]. This occurs as an excessive external force acting on the fruit surface, when it collides with a rigid plate or another fruit [8]. Bruising can happen during handling fruit containers from the field to the packaging line, and also during packaging by receiving impact from a rigid surface [9]. Accordingly, as a research interest, prediction of damage, stress distribution and deformation of biological materials exposed to external forces is highly important to agricultural mechanization. Quantification of deformation and internal stresses is a very complicated task, since they are caused by external forces and depend on the cell structure of fruits and vegetables [10]. Pendulum experiments or drop test are two classical ways for simulating and investigating impact damages on fruits [11,12]. However, the information provided by these experiments is not complete enough to be used in guiding a process and equipment design [13].

Numerical methods are powerful tools used for simulating and investigating material behavior with given boundary conditions. Since analytical methods for stress can be adopted for only a few simple cases, they are not widely used [14]. Recent technologies, along with advances in computer and software industries, allow engineers to virtually solve highly difficult problems using computer aided design (CAD) and numerical methods without developing and testing prototypes [15]. The real-life problems of agricultural engineering are usually complicated problems that can be solved only by numerical methods [16]. Finite Element Method (FEM) is one of these methods. The FEM approach is the numerical computation of an estimate for a differential or integral equation that is hard to solve analytically. FEM divides a complex problem into smaller sections to solve its simplified equations. Partial solutions are then summarized to obtain approximates [17].

Some researchers have applied FEM to simulate the drop test of fruits like apples [10], peaches [16], and tomatoes [18]. These efforts supported FEM applicability as a computational tool for determining a number of fruit properties and their deformation behavior. Pears are vulnerable to mechanical damage due to their soft texture and thin skin. Although there are a few analytical studies on mechanical properties of pears [19,20], there are limited numerical or simulation studies in this regard. Therefore, this study aimed at (1) FEM-analyzing the stress/strain distribution of pear exposed to the drop scenario, (2) measuring the overall contact force between fruit and impact material, and (3) evaluating the effect of impact surface material, and drop orientation on the magnitudes of these three parameters.

2. Materials and methods

2.1. Fruit materials

Shekari variety pears (*Pyrus communis* L.) were manually harvested from an orchard in Alborz, Iran. The fruits were at

their commercial maturity on September 18, 2015. Pears were picked based on their size and skin color. In fact, the fruits were harvested when they reached commercial size and their skin was all light yellow. Samples were taken to a laboratory 20 km away from the orchard in a standard temperature-controlled truck. In the laboratory, fruits with no visible defects or decay were selected for experiments among which 20 samples were randomly selected for physical and moisture content (MC) measurements. They were then washed with tap water and their external moisture was wiped with a dry fabric. Their mass was weighed by an analytical balance (BP 160P, Sartorius, Germany), whereas their three perpendicular diameters were measured by a digital caliper (CD-6CSX, Mitutoyo, Japan). Using the water displacement technique (Archimedes' principle), the volume of samples was determined. With mass and volume being determined, their density was then calculated as the mass to volume ratio of each sample [21]. The initial MC was determined gravimetrically by placing samples in an oven at 105 °C and 1 atm for 24 h [22]. MC was measured three times and the mean value was reported. During the experimentation (2 days), the rest of the fruits (40 samples) were also cleaned and stored at optimal conditions (4 °C, 75% relative humidity). Fruits were kept at room temperature (nearly 2 h) before each experiment [23]. Similarly, all analyses were performed at room temperature (20 ± 1 °C).

2.2. 3D solid modeling

In reality, pears have a complicated asymmetric shape, which makes it difficult to develop a 3D solid model. The 3D surface model for objects of complicated shapes is generated from the beams projected from a 3D scanner and the beam reflection off the pear surface. In this study, a non-contact 3D scanner (3D scanner advanced, RangeVision, Russia) was thus used to generate pear surface model. The surface model was then processed as a 3D solid model in CATIA V5 software (Fig. 1).

2.3. Mechanical properties

To determine mechanical properties of pear, compression tests were conducted using a universal testing machine (H5KS, Tinius Olsen, UK), with a 1 kN load cell. An aluminum cylindrical probe with a round end and 8 mm diameter was used to compress the samples at a constant speed of 7 mm/min [16]. Pears were cut in half along their stem-calyx axis. Each half was placed separately at the center of a fixed plate with its stem-calyx axis being horizontal (Fig. 2a). Having the compression speed and time, sample deformation was determined to draw force-deformation curves for each sample. The compression data were processed and force-deformation curves were generated and recorded by Qmat 4.55-Dongle.:4959 software package. Samples were exposed to compressive loading until reaching their failure point. Deformation energy was directly determined as the total area under the force-deformation curve from zero deformation until the failure occurs [24]. Stress and strain at the failure point were determined using the equations in Kabas et al. [18] Young's modulus was calculated using the Hertz theory,

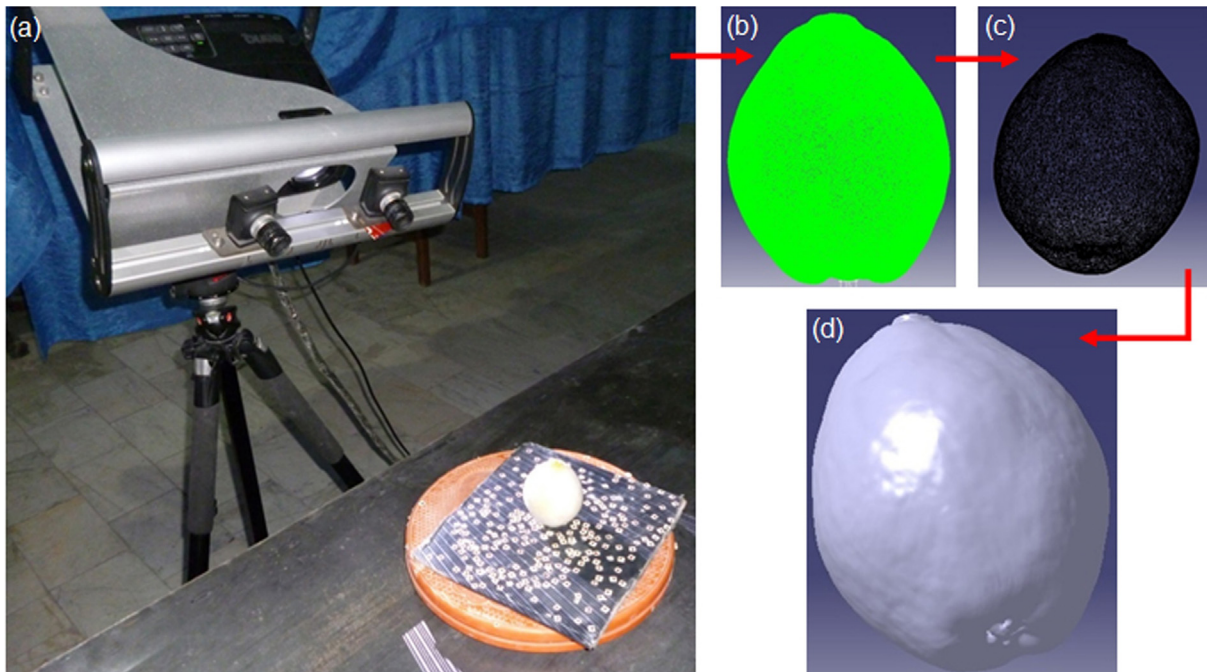


Fig. 1 – The procedure of creating a 3D-digital model pear from a real pear: (a) 3D scanning; (b) generating point clouds; (c) mesh generation; and (d) creating a solid model.

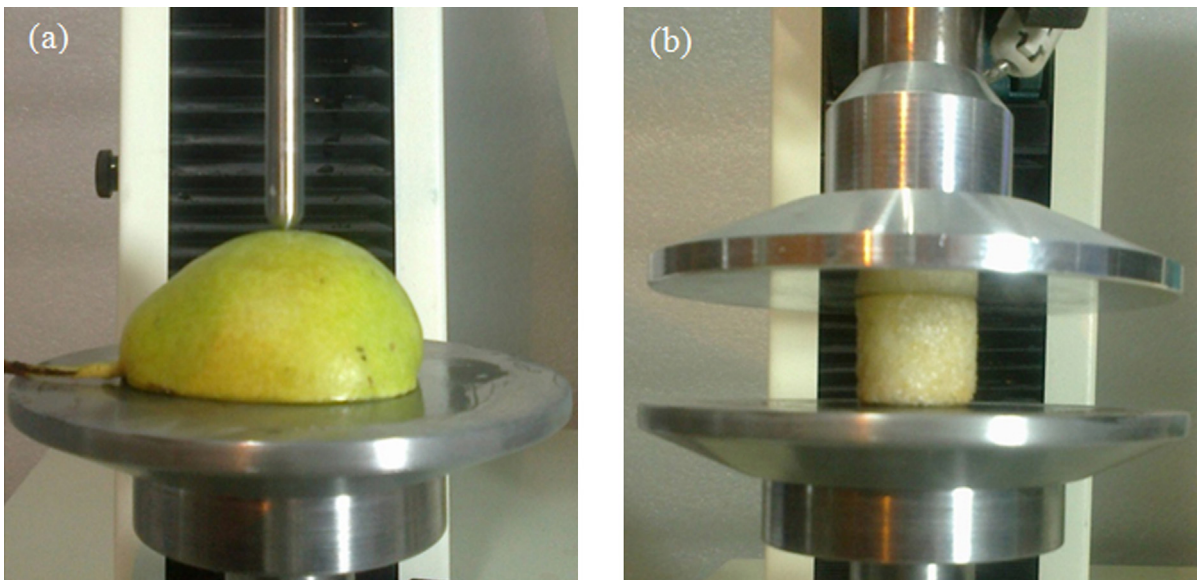


Fig. 2 – (a) Halved section of the pear under compression of a convex-tip probe and (b) a cylindrical sample of the pear tissue under axial loading.

assuming loading as a spherical indenter on a curved surface [25]:

$$E = \frac{0.338 K_u^{\frac{3}{2}} F(1 - \mu^2)}{D^{\frac{3}{2}}} \left(\frac{1}{R_u} + \frac{1}{R'_u} + \frac{4}{d} \right)^{\frac{1}{2}} \quad (1)$$

where E is the apparent modulus of elasticity or Young's modulus (Pa), F is the compressive force applied on samples (N), D is the compressive deformation (m), μ is Poisson's ratio (dimensionless), R_u and R'_u are the minimum and maximum radii of surface curvature at the contact point, respectively

(m), d is the diameter of the spherical indenter (m), and K_u is the constant for the upper convex surface. The radius of curvature was measured at the contact point by a curvature meter [26]. K_u was determined from Table 1 using linear interpolation once the value of $\cos \theta$ was determined from the following relation [25]:

$$\cos \theta = \left(\frac{1}{R_u} - \frac{1}{R'_u} \right) / \left(\frac{1}{R_u} + \frac{1}{R'_u} \right) \quad (2)$$

Table 1 – Value of K_u for various values of θ (degrees) [25].

θ (°)	50	55	60	65	70	75	80	85	90
$\cos \theta$	0.6428	0.5736	0.5000	0.4226	0.3420	0.2588	0.1736	0.0872	0.0000
K_u	1.198	1.235	1.267	1.293	1.314	1.331	1.342	1.349	1.351

where θ is the angle between the normal planes containing the principle curvatures.

To measure pears' Poisson's ratio the method described in Bentini et al. [27] was used. In this method, a 25 mm-long cylindrical specimen with a 25 mm diameter was taken from the inner homogenous tissue and was compressed between two parallel flat plates in one axis until reaching a certain deformation level. The compression was done at the cross-head speed of 7 mm/min (Fig. 2b). The before-mentioned universal testing machine was used for this purpose.

Poisson's ratio is defined by Eq. (3):

$$\mu = \frac{\varepsilon_a}{\varepsilon_r} \quad (3)$$

where ε_a is the absolute value of loading direction strain (axial strain) and ε_r is the radial strain:

$$\varepsilon_a = \left| \frac{\Delta L}{L_0} \right| = \left| \frac{L_f - L_0}{L_0} \right| \quad (4)$$

$$\varepsilon_r = \frac{\Delta D}{D_0} = \frac{D_f - D_0}{D_0} \quad (5)$$

where L_0 is the original length prior to compression, L_f is the final length after compression, ΔL is the length deformation, D_0 is the original diameter prior to compression, D_f is the final diameter after compression, and ΔD is the diameter deformation. Each mechanical test was performed in twenty replications according to the ASABE standard's requirements [25].

2.4. Drop-test simulation

Drop test studies focus on the effect from collision between a part or an assembly and a rigid or flexible plate [16]. Drop tests were simulated here in ABAQUS FEA software. This software application automatically determines impact and gravitational loads. There were no other loads or constraints. ABAQUS FEA calculates the velocity (V) of impact using the free fall equation, $V = (2gh)^{1/2}$, where g is the gravity (m/s^2) and h is the drop height (m). For dynamic analysis, the equation of motion for system with multiple degrees of freedom under external loading is expressed as follows [28]:

$$[M]\{\ddot{H}\} + [C]\{\dot{H}\} + [K]\{H\} = \{P\} \quad (6)$$

where M is the mass matrix, \ddot{H} is the acceleration vector, C is the damping matrix, \dot{H} is the velocity vector, K is the stiffness matrix, H is the displacement vector, and P is the external force vector.

In the simulation, a rigid body falls along gravity until colliding with a rigid or flexible plane (without any rotation before the initial impact). In a drop test, damping, friction and plastic deformation are the main mechanisms by which energy loss occurs. The coefficient of friction between contact surfaces was defined as an important parameter of the simulation. The dynamic coefficients of friction between

pears and steel, wood (pine), Perspex and rubber surfaces were determined. These coefficients were measured using a friction device, developed by Tsang-Mui-Chung et al. [29] and modified by Chung and Verma [30]. The dynamic coefficient of friction (μ_d) with a torque acting on the sample can be determined using the following formula [31]:

$$\mu_d = \frac{T_m}{Wq} \quad (7)$$

where T_m is the mean value of torques during the rotation of the disk (Nm), W is the fruit weight acting on the rotating surface (N), and q is the length of the torque arm (m). The friction tests were repeated three times.

A dynamic analysis solver is required for drop tests, and software performs this analysis based on the direct-time integration method. This technique is computationally intensive but numerically stable that can be applied to solve dynamic analysis problems [10]. In practice, all responses cannot be obtained in simulations. Due to limitations and uncertainties caused by factors such as materials, fluids and dynamic environment conditions, assumptions should be made to gain approximate solutions [32]. Similar limitations led us to assume that pear, together with its skin, was a whole solid. Therefore, an isotropic material model was developed for the FEM simulation. Fruits' free fall on hard surfaces made of steel, wood (pine) and Perspex is highly prevalent during their mechanized handling [33]. On the other hand, using flexible materials like rubber for covering rigid surfaces is practiced in several leading agricultural machinery manufacturers. Therefore, in this study a few rigid and flexible sheets made of these materials were considered as the impact surfaces, with their properties given in Table 2. The effect of drop orientation (vertical or horizontal) on the impact surface was also analyzed (Fig. 3). The damaging height for pear was determined through the following equation [34]:

$$h = \frac{(1.5)^5 \sigma \varepsilon R^3}{mg} \quad (8)$$

where h is the damaging height (mm), σ represents the mean stress (N/mm^2), ε is elongation (%), R is the radius of curvature (mm), m denotes the sample's mass (kg), and g is the gravitational acceleration (m/s^2).

Table 2 – Impact surface material properties.

Impact material	Properties		
	Poisson's ratio	Density (g/cm^3)	Elastic modulus (N/mm^2)
Perspex	0.38	1.24	2350
Steel	0.30	7.85	200000
Wood	0.34	0.32	8890
Rubber	0.49	1.00	100

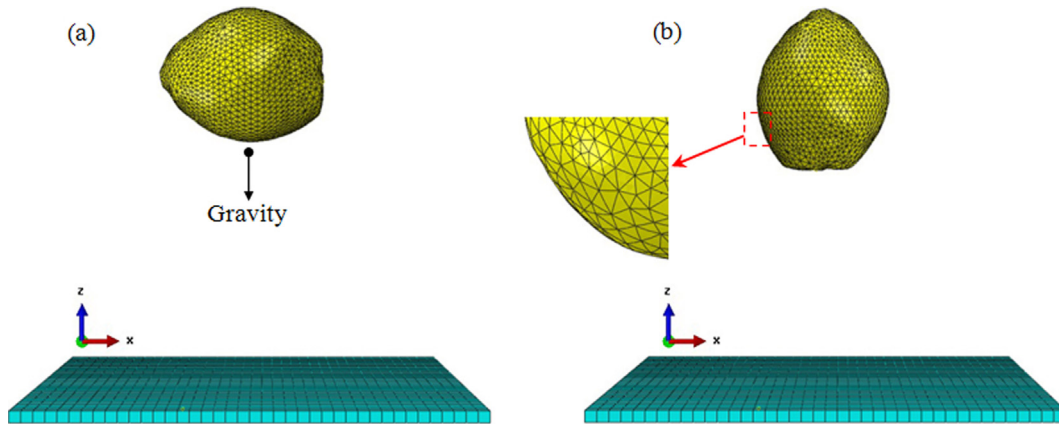


Fig. 3 – Drop orientations of pear: (a) horizontal drop; and (b) vertical drop.

Meshing is one of the most important steps in FEM, where a model is divided into smaller parts called elements. This means that a system with a finite degree of freedom replaces another system with an infinite degree of freedom [35]. For simulation purposes, a 3D model of pear was meshed using a 10-node modified quadratic tetrahedron element (C3D10M). This element was selected due to its high accuracy and excellent performance in contact analysis [36]. A total number of 33198 elements and 38917 nodes were generated after meshing the solid model. A major objective of FEM simulations is to find the largest stresses and strains produced in agricultural products following collision with different surfaces. Therefore, a number of steps were defined in ABAQUS to obtain these parameters. Indeed, in the collision of horticultural product with any surface, the detection of consequent maximum stress, strain and contact force is highly important, because these maximums correspond to the condition when the maximum damage might occur. Knowing these values, one can predict the size of the damage on fruits. These types of collisions are divided into two phases: rising and falling. The former ends once the maximum value is achieved. The latter, however, immediately starts after the rising phase and continues until reaching zero. Therefore, the solution time was selected based on the certainty in reaching the maximum values of the above-mentioned parameters. The solution time following an impact on the rubber surface was 8500 microseconds (μ s) and for the other studied surfaces was 5000 μ s. A total of 51 steps were selected in pre-processor operations for simulating free fall on a rubber surface, and 30 steps were set for the other surfaces after the first impact. The Von Mises plasticity model was incorporated. The strain distributions and contact forces (resultant normal and tangential forces) were also obtained for each step. Experimentally, the contact forces are difficult to measure. However, they are easy to represent in ABAQUS program.

3. Results and discussion

3.1. Physical and mechanical properties of pears

The average values of measured physical properties of studied pear fruits, i.e., major diameter, intermediate

diameter, minor diameter, weight, volume and density were 60.51 ± 4.77 mm, 52.67 ± 1.79 mm, 51.29 ± 2.23 mm, 77.86 ± 6.13 g, 85.56 ± 5.11 cm³, 0.91 ± 0.02 g/cm³, respectively. The mechanical data of the fruits were: 107.82 ± 7.25 N·mm (deformation energy), 0.798 ± 0.031 N/mm² (failure stress), 0.275 ± 0.041 (failure strain), 1.693 ± 0.082 N/mm² (Young's modulus), and 0.410 ± 0.011 (Poisson's ratio). The average dynamic coefficient of friction on four different surfaces, namely, steel, wood, Perspex and rubber was found to be 0.332 ± 0.029 , 0.278 ± 0.020 , 0.236 ± 0.005 and 0.514 ± 0.044 , respectively. These properties were found at specific MC of about 82.38% wet basis. From the results of compression study, a dropping test was simulated for a typical pear sample and its behavior was investigated for a dropping from 207.22 mm high.

3.2. Effect of impact surface material and drop orientation on stress

Magnitudes of the generated stresses in the inner structure of pear at different steps of its horizontal fall on the steel object are shown in Fig. 4. The trend variations in maximum stress at different steps of horizontal fall on the steel plate are clearly

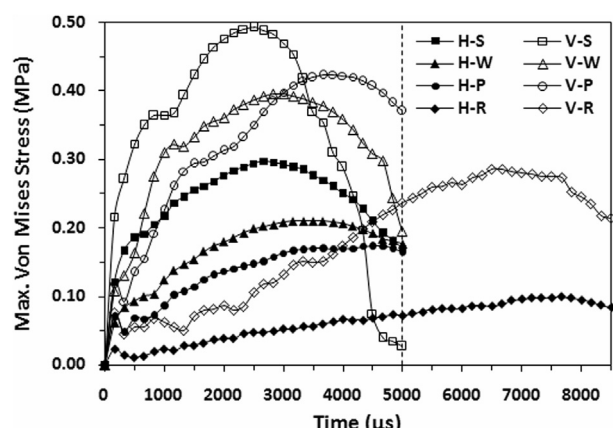


Fig. 4 – Stress-time diagram for the collision of pear to rigid and flexible objects: (H) horizontal; (V) vertical; (S) steel; (W) wood; (P) Perspex; (R) rubber.

shown. Results of maximum stresses generated by pear free-fall on a steel plate in horizontal orientation can be classified into 3 sections. The first section is related to the large increase in stress magnitude from step 1 to 500 µs after impact (step 3), the second one is related to the mild increase in stress magnitude from step 3 to 2666 µs after impact (step 16), and the third section involves a uniform decrease from step 16 to onwards. This behavior in the stress plot was in complete agreement with the results obtained by previous researchers [37]. FEM simulation results showed that, in horizontal fall on a fixed steel plate, the maximum Von Mises stress (0.297 MPa) occurred on the inner structure at step 16 (Fig. 5). A graphical representation of stress distribution on pear sample under free fall conditions on a steel fixed plate at 2.016 m/s is shown in Fig. 5, spanning the period from the impact moment (i.e. when the first stress value is obtained at step 1) until 5000 µs later (step 30). Through the horizontal collision of pear with the steel plate, the maximum stress within the area of impact with the rigid plate can be obtained. Fig. 5 shows the propagation of the stress wave from the impact point towards the inner parts of the sample. This is in complete agreement with the results reported by other authors [16,18].

FEM simulations of vertical falling on the steel plate showed that the maximum Von Mises stress occurred on the inner structure (0.493 MPa) at step 15 (Fig. 6). Fig. 6 shows the manner of stress distribution on pear when the sample collides vertically with the steel plate. Cross-sectional views of stress distribution for pear colliding vertically with the steel plate show that, like the horizontal fall, maximum Von Mises stress concentration is at the impact point, and the stress extends from the impact point towards the center of sample (Fig. 6). Maximum stress magnitudes generated on the inner structure of pear at different vertical fall steps on the steel plate are given in Fig. 4. Variations in stresses generated in sample vertically colliding with the steel plate can be classified into 3 sections. The first section is related to the large increase in stress magnitude from step 1 to 833 µs after impact (step 5), the second one is related to the mild increase in stress magnitude from step 5 to 2500 µs after impact (step 15), and the third section involves a continuous decrease from step 15 to onwards. Results from FEM simulations revealed that, following vertical collision with the steel plate, larger stresses are generated inside fruit than those generated by horizontal collision. This difference can be due to the

geometric shape of sample and the contact area between fruit and contact surface.

FEM results showed that, in horizontal drop on a fixed wooden plate, the maximum Von Mises stress (0.210 MPa) was created on the inner structure of pear at step 20 (Fig. 7). Fig. 7 shows the stress distribution on pear when the sample collides horizontally with the wooden plate. Cross-sectional views of stress distribution for pear colliding horizontally with the wooden plate illustrate that the maximum Von Mises stress concentration is at the impact point, and the stress extends from this point towards the edges. Fig. 4 shows the graphical representation of changes in maximum stress values of the inner pear structure at different fall steps in the horizontal orientation on a wooden surface. With regard to this figure, stress variations of pear can be divided into two increasing and declining phases following its collision with a wooden object. During the increasing phase, the maximum generated stress on the inner texture reached from 0.061 MPa at step 1 to 0.210 MPa at step 20. Whereas, in the declining phase following step 20, the maximum stress reached 0.177 MPa at step 30. This behavior in the stress plot was in good agreement with the results obtained by Celik et al. [10].

FEM simulations for the vertical collision of sample with the fixed vertical wooden plate show that the maximum Von Mises stress occurred on the inner structure (0.395 MPa) at step 17 (Fig. 8). Fig. 8 shows the distribution of stress wave for pear following its vertical collision with the wooden plate. According to Fig. 8, upon vertical collision of pear with the wooden plate, the maximum stress occurs at the impact point, and the stress distribution wave propagates from this point towards the inner layers of sample. Variations in stresses generated by vertical fall on wood against time are shown in Fig. 4. Variations in stresses caused by vertical collision of the modeled pear with a wooden plate show an increasing trend followed by a declining phase. Accordingly, during its increasing phase, the maximum stress started from 0.108 MPa at step 1 and reached 0.395 MPa at step 17, from which point it enters its declining phase and drops to 0.194 MPa at step 30. Results from FEM simulations showed that, following vertical collision with the wooden plate, similar to the steel plate scenario, larger stresses were generated inside fruit than those generated by horizontal collision.

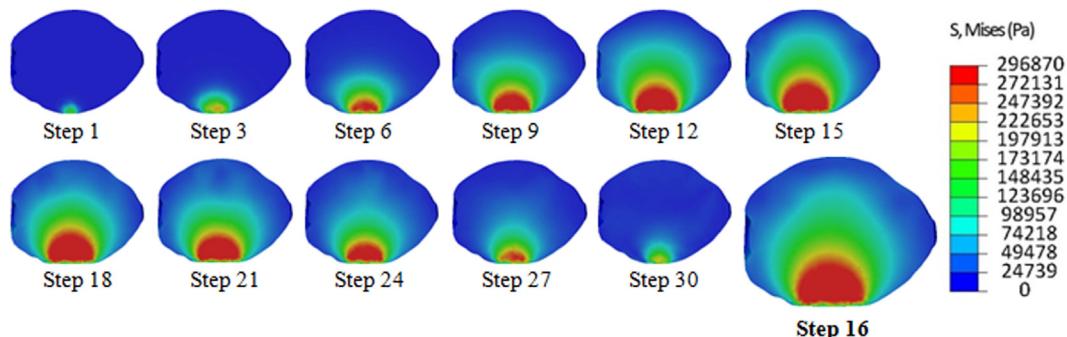


Fig. 5 – The stress distribution in the inner structure of pear at different time steps after its horizontal impact on a steel surface.

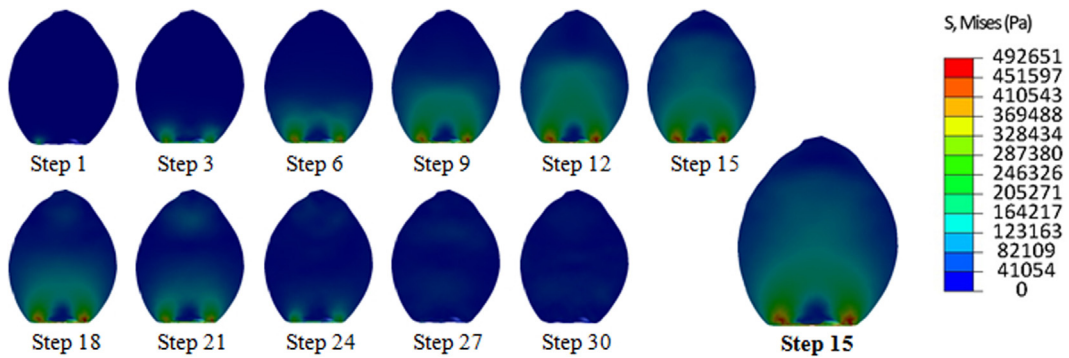


Fig. 6 – The stress distribution in the inner structure of pear at different time steps after its vertical impact on a steel surface.

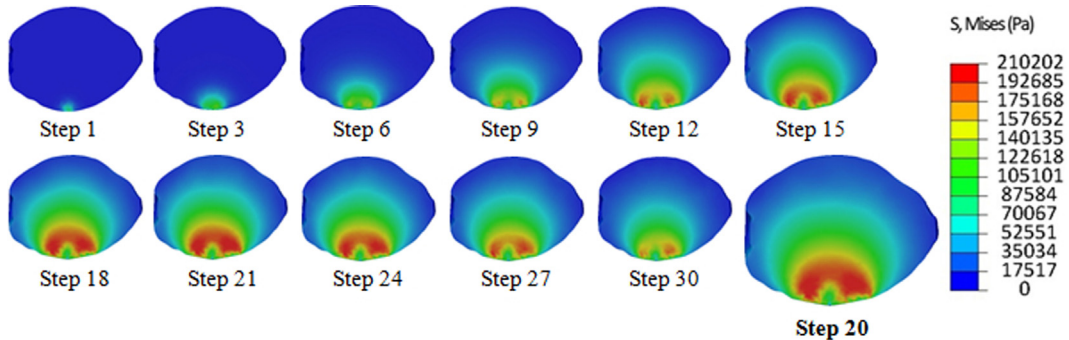


Fig. 7 – The stress distribution in the inner structure of pear at different time steps after its horizontal impact on a wooden surface.

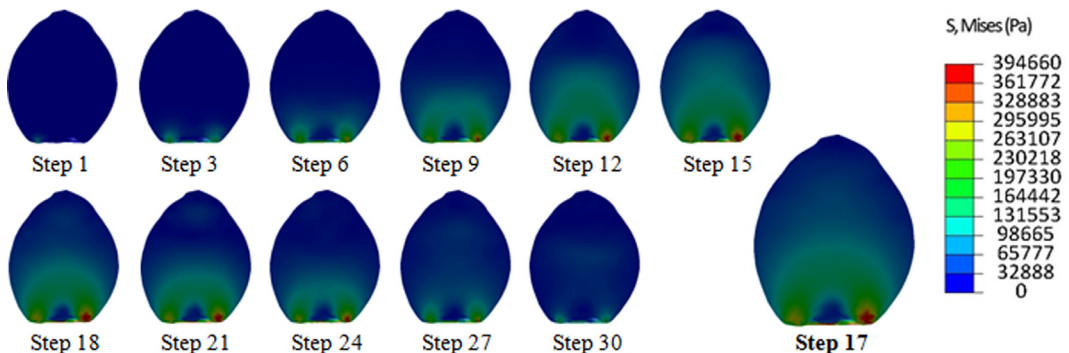


Fig. 8 – The stress distribution in the inner structure of pear at different time steps after its vertical impact on a wooden surface.

FEM simulation results showed that, in horizontal fall on a fixed Perspex plate, the maximum Von Mises stress (0.174 MPa) occurred on the inner structure at step 27 (Fig. 9). Fig. 9 shows stress distribution on pear when the sample collides horizontally with a plate made of Perspex. Cross-sectional views of stress distribution for pear colliding horizontally with the Perspex plate show that the maximum Von Mises stress concentration is at the impact point, and the stress wave propagates from the impact point towards the center of sample (see Fig. 9). The variation of maximum stress inside the pear structure within a few seconds after horizontal fall on a Perspex plate are shown in Fig. 4. FEM simulations for the vertical collision of sample with the fixed

Perspex plate show that the maximum Von Mises stress occurred on the inner structure (0.424 MPa) at step 23 (Fig. 10). As shown in Fig. 10, similar to the results obtained from the simulated fall of the modeled pear on the steel and wood surfaces, the maximum stress from collision between Perspex plate and pear along its longitudinal axis occurred at the impact point, and then the stress wave propagated towards the center of sample. It was seen in Fig. 4 that the stress increased in a sample colliding vertically with the Perspex plate until reaching its greatest value. Additionally, similar to other analyses, the vertical collision of sample with the Perspex plate resulted in larger stresses in the fruit than those generated by its horizontal collision.

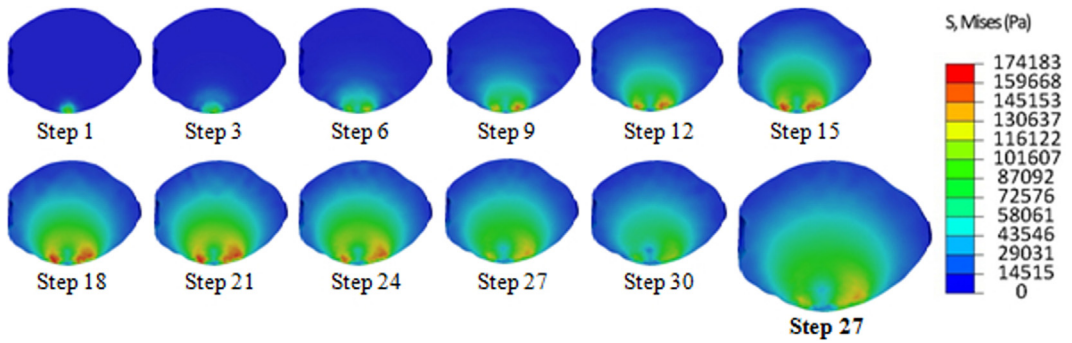


Fig. 9 – The stress distribution in the inner structure of pear at different time steps after its horizontal impact on a Perspex surface.

The output of numerical computations was a non-uniform stress distribution in pear structure generated following horizontal collision with the rubber surface (Fig. 11). However, the highest stress concentration was around the impact point. In this collision, the largest stress (0.099 MPa), which was considerably lower than stresses produced in collision with other surfaces, occurred at step 46 (7666 μ s after impact). In the case of vertical impact, the stress was also distributed non-uniformly, as shown in Fig. 12. Additionally, the stress concentration can be seen around the impact location at all steps. The largest stress (0.286 MPa) occurred at step 39 (6500 μ s after impact). The maximum stress magnitudes generated in sample following collision along both axes with the rubber surface is shown in Fig. 4 against time. From this figure, it is found that in both orientations, during the early moments of impact, this parameter had oscillatory variations, which was probably due to the elasticity of the rubber surface.

In sum, FEM results suggest that, regardless of the collision surface type, fruit fall either on a rigid or a flexible surface along its vertical axis would lead to larger stresses than falling along its horizontal axis. Additionally, for both fall directions, the largest and smallest stresses were found in the case of the fruit dropping on steel and rubber surfaces, respectively. Horizontal collision of pear with a wooden surface led to larger stresses on its inner tissue, when compared to the Perspex surface. In contrast, vertical collision with Perspex surface produced larger stresses than collision with the wooden plate.

In both vertical and horizontal directions, the shortest and longest times to produce the maximum stress belonged to the steel and rubber surfaces, respectively. Despite the larger stresses produced from falling on vertical axis on all four surfaces, these stresses reach their maximum value in a shorter time period than falling on horizontal axis. These differences are due to the geometric characteristics of fruit and physical and mechanical properties of the impact surfaces. This information can be useful during designing harvest, handling, sorting, packaging and processing machinery in order to reduce losses and improving quality. For example, for selecting a mechanism that aligns pears along their horizontal axis on conveyors in packaging lines, it is necessary to take account of these results to avoid internal damages. Because, damage is essentially a product of the stresses produced during loading within samples [38]. Based on these results, engineers should follow the following recommendation while designing an intelligent, efficient system to avoid post-harvest damages: In cases where steel cannot be removed from the structure of equipment that have collision with pears, it is suggested to avoid impact along their vertical axis and in a good design. It is also recommended that rigid surfaces are covered with rubber sheets to significantly reduce unwanted impact-induced stresses on fruits. Similarly, horizontal contact/impact should be provided for equipment that uses wooden or Perspex surfaces, in order to minimize dynamically generated stresses.

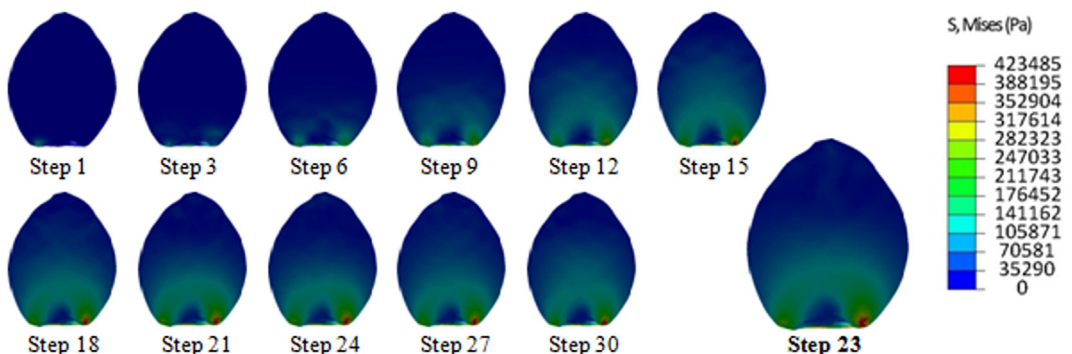


Fig. 10 – The stress distribution in the inner structure of pear at different time steps after its vertical impact on a Perspex surface.

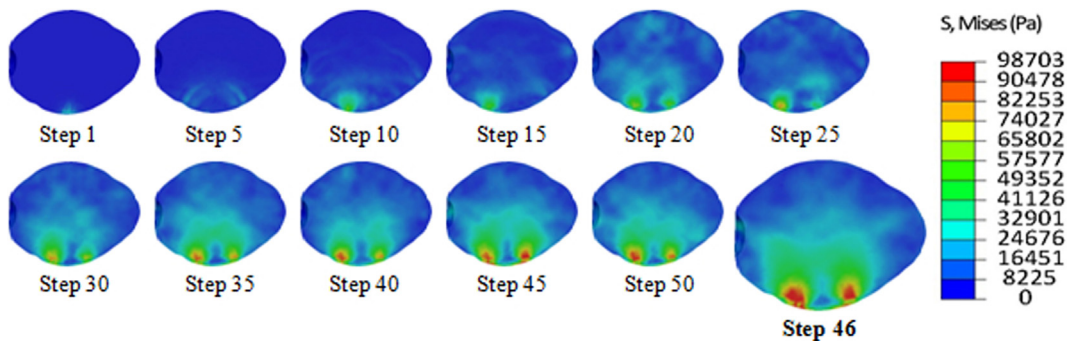


Fig. 11 – The stress distribution in the inner structure of pear at different time steps after its horizontal impact on a rubber surface.

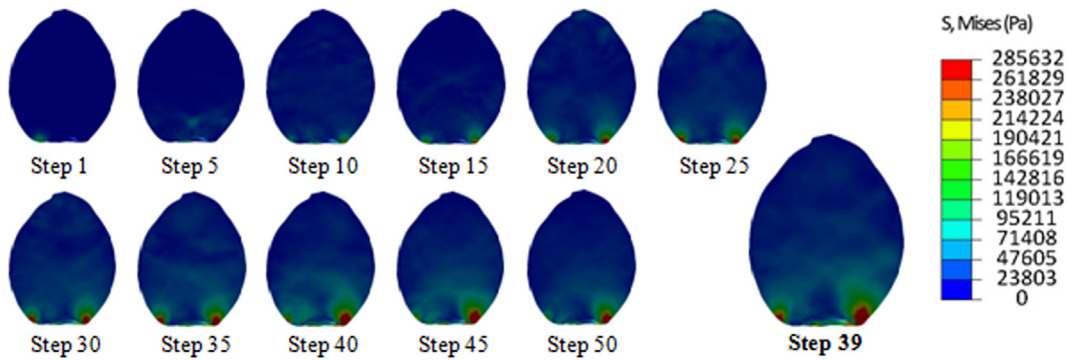


Fig. 12 – The stress distribution in the inner structure of pear at different time steps after its vertical impact on a rubber surface.

3.3. Effect of impact surface material and drop orientation on strain

The largest magnitudes of strains produced in the internal structure of pears at different stages of their horizontal fall on the steel plate are depicted in Fig. 13. Maximum strain variations at different steps of horizontal fall of pear on the steel plate is similar to variations in maximum stress. Maximum strains generated by pear free-fall on a steel plate in horizontal orientation can be classified into 3 sections. The first section is accompanied by a large increase in strain from step 1 to 666 μ s after impact (step 4); the second one showed a mild increase in strain magnitude from step 4 to 2833 μ s after impact (step 17), followed by a continuous decrease from step 15 to step 30. FEM simulation results showed that, in horizontal fall on a fixed steel plate, the maximum strain (0.157) occurred on the inner structure at step 17 (Fig. 14). Strain distribution in pear falling on its horizontal axis on a fixed steel plate from the time impact to 5000 μ s afterwards is shown in Fig. 14. Through the collision of pear with the steel plate, the maximum strain was observed at the impact area, and the distribution trend of the strain wave is from the impact point towards the inner parts of the sample, as shown in Fig. 14. Visual evaluation of Figs. 5 and 14 suggests that the largest strains occurred at the location of the largest stresses.

FEM simulations of vertical falling on the fixed steel plate show that the maximum strain occurred on the inner structure (0.219) at step 14 (Fig. 15). The distribution of strain

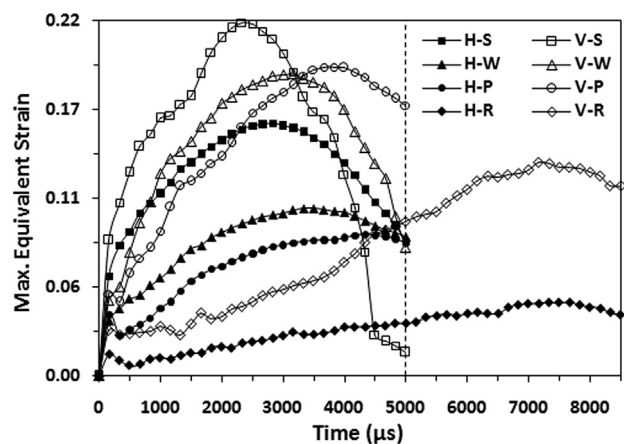


Fig. 13 – Strain-time diagram for the collision of pear to rigid and flexible objects: (H) horizontal; (V) vertical; (S) steel; (W) wood; (P) Perspex; (R) rubber.

within the inner structure of pear, when falling on its longitudinal axis on the steel plate, is shown in Fig. 15. The strain distribution pattern is similar to the stress distribution within a sample colliding with the steel plate along its vertical axis. In fact, the maximum strain concentration is in the impact area, and it develops towards the center of the sample (see Fig. 15). Maximum strain magnitudes inside the sample at step 30 after vertical collision with the steel plate are also

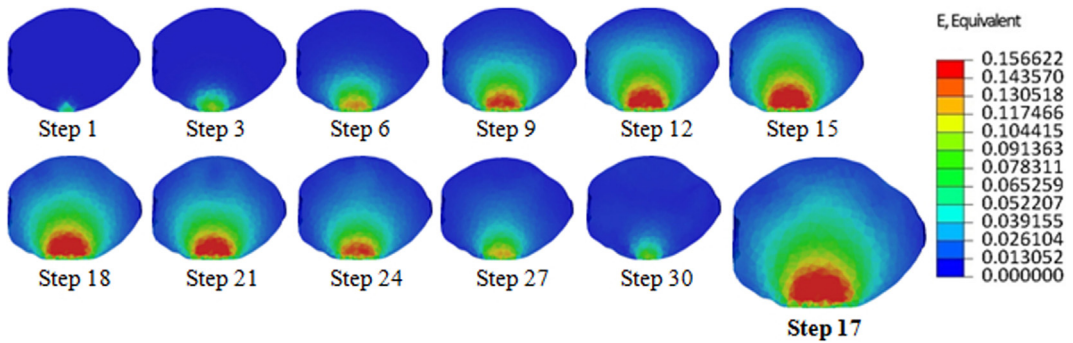


Fig. 14 – The strain distribution in the inner structure of pear at different time steps after its horizontal impact on a steel surface.

shown in Fig. 13. Strain variations are divided into three segments for a sample colliding vertically with a steel plate. The first segment included a large increase in strain from step 1 to 1000 μ s after impact (step 6). The second segment showed a mild increase in strain from step 6 to 2333 μ s after impact (step 14), and the third segment was accompanied by a decrease from step 14. Regarding the effect of drop orientation, the largest strain occurred during vertical collision of sample with the steel plate, since larger stresses occurred in this case.

FEM analysis results showed that, in horizontal fall on a fixed wooden plate, the maximum strain (0.104) occurred on the inner structure at step 20 (Fig. 16). Strain distribution for horizontal collision of pear with the wooden surface is shown in Fig. 16. In this case, the maximum strain concentration occurs near the impact point, and its magnitude gradually decreases towards edges. Strain produced by horizontal drop on the wooden plate increases from the impact moment to 3333 μ s after impact, and then it follows a decreasing trend (Fig. 13). During the vertical collision with the wooden plate, FEM simulations show that the maximum strain occurred on the inner structure (0.188) at step 19 (Fig. 17). Strain distribution wave after vertical collision with the wooden plate is shown as a function of time in Fig. 17. Similar to stress distribution, the maximum strain also occurred at the impact point, and the strain distribution wave extends from that impact point towards the inner layers of pear (see Fig. 17). Maximum strain variations against time elapsed from vertical collision with the wooden plate are shown in Fig. 13.

According to this figure, the maximum strains ranged from 0.047 at the impact moment to 0.188 at 3166 μ s after impact. Immediately from this point on, this parameter decreases until reaching 0.080 at 5000 μ s after impact. FEM-based computations showed that, similar to the sample's behavior to the collision with steel, the internal tissue strains produced in vertical collision with the wooden plate were also larger than those produced from horizontal collision on this plate.

FEM simulation results showed that, in horizontal fall on a fixed Perspex plate, the maximum strain (0.088) occurred on the inner structure at step 26 (Fig. 18). The strain distribution in horizontal fall of pear on a Perspex surface is shown in Fig. 18. A closer look at this figure revealed that maximum strains were concentrated at the impact area. Note that, unlike strain distributions from collision with wooden and steel plates, strain was distributed non-uniformly within the inner structure of pear falling on the Perspex surface. The maximum strain magnitudes from falling horizontally on this surface are plotted as a function of time in Fig. 13. During the vertical collision with the Perspex plate, FEM simulations showed that the maximum strain occurred on the inner structure (0.192) at step 23 (Fig. 19). Frames in Fig. 19 are snapshots at different times following the first impact, in which the maximum strain concentration was expectedly at the impact point, and the strain wave moved towards the sample center. The increasing and declining trends of strain in sample colliding vertically with the Perspex surface are shown in Fig. 13. In collision with the Perspex surface, the larger strain was also associated with the vertical impact.

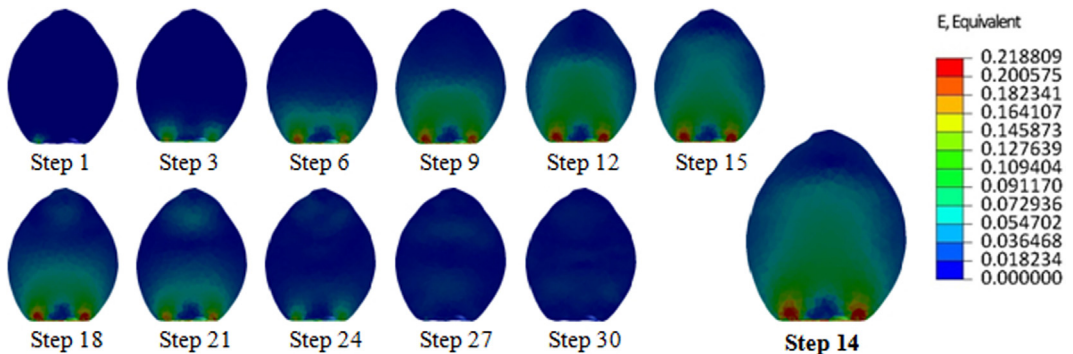


Fig. 15 – The strain distribution in the inner structure of pear at different time steps after its vertical impact on a steel surface.

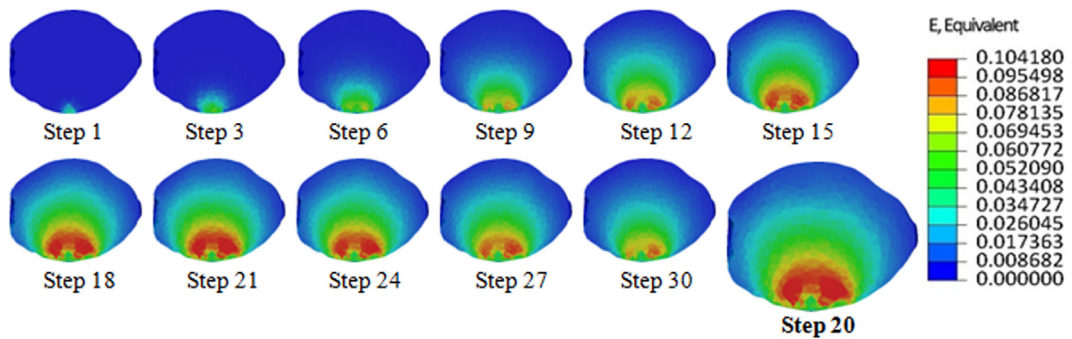


Fig. 16 – The strain distribution in the inner structure of pear at different time steps after its horizontal impact on a wooden surface.

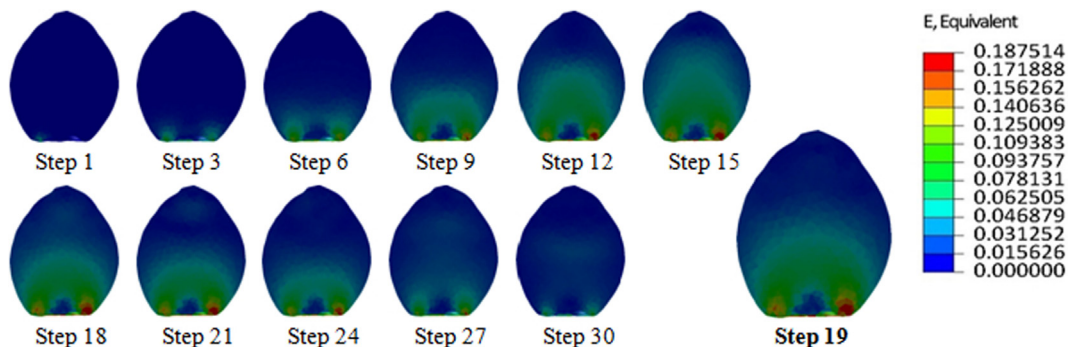


Fig. 17 – The strain distribution in the inner structure of pear at different time steps after its vertical impact on a wooden surface.

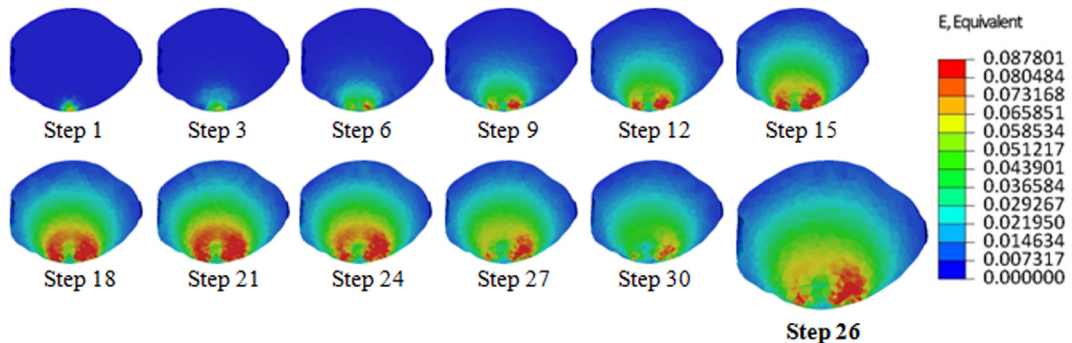


Fig. 18 – The strain distribution in the inner structure of pear at different time steps after its horizontal impact on a Perspex surface.

FEM analysis results showed that the largest strain (0.046) from the horizontal collision of fruit with the rubber surface occurred after 7666 μ s (step 46) from the impact, as shown in Fig. 20. However, for the vertical collision, the largest strain (0.132) occurred in a shorter time from the impact (7166 μ s), as shown in Fig. 21. The strain distribution was non-uniform under dynamic loading, and the largest strains were observed around the point of impact (Figs. 20 and 21). According to the strain-time curves in Fig. 13, the temporal variation of maximum strain inside the pear,

imposed by collision from both orientations on the rubber surface can be divided into three distinct regions: (i) an immediately after impact region with highly fluctuations in maximum strain, which is probably related to high-energy absorption of rubber; followed by (ii) a rising strain region and finally (iii) a region with falling strain. FEM simulation results for strain were in agreement with those for stress simulation. For all studied surfaces, the highest and lowest strains occurred in vertical and horizontal impacts, respectively.

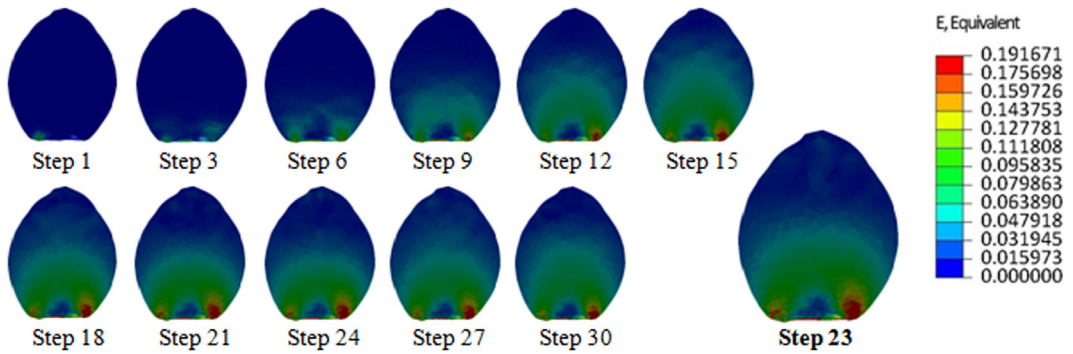


Fig. 19 – The strain distribution in the inner structure of pear at different time steps after its vertical impact on a Perspex surface.

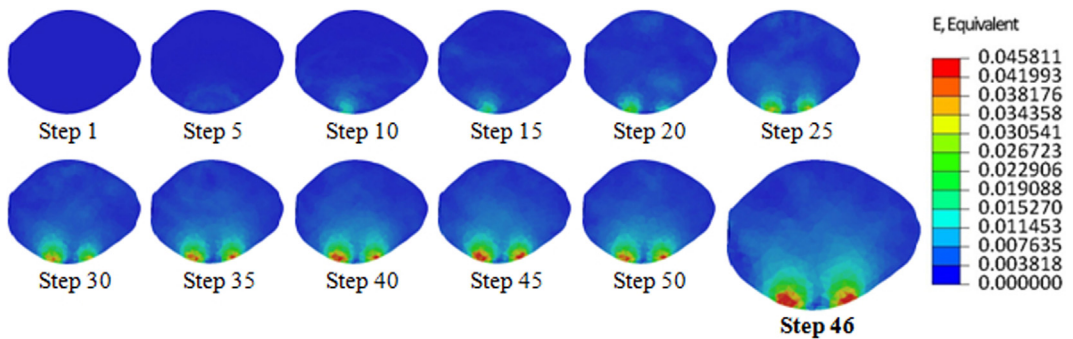


Fig. 20 – The strain distribution in the inner structure of pear at different time steps after its horizontal impact on a rubber surface.

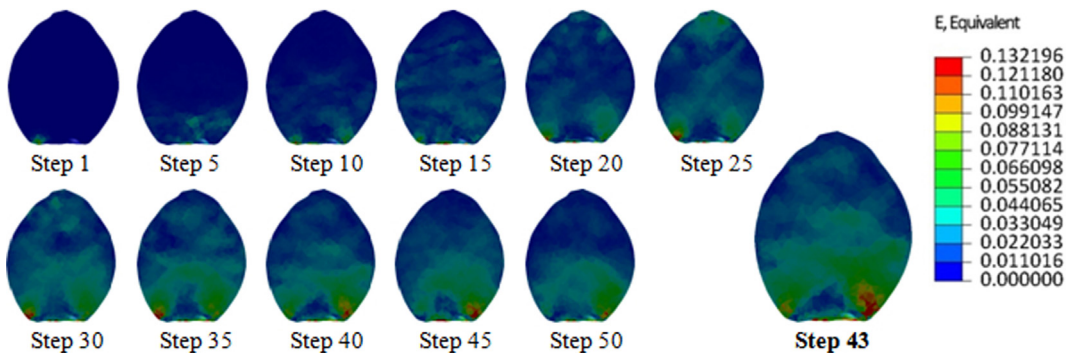


Fig. 21 – The strain distribution in the inner structure of pear at different time steps after its vertical impact on a rubber surface.

3.4. Effect of impact surface material and drop orientation on contact force

Contact forces resulted from pear collision in both orientations with steel are given in Fig. 22. As shown in this figure, the maximum contact force from horizontal and vertical impacts reached 150.37 N (step 17) and 154.41 N (step 14), respectively. Following these steps, samples bounce as a reaction to the steel surface. Compression tests revealed that the highest force required for pears to reach a biological yield point was 38.79 N, which considerably lower than the forces acting on fruit following collision in both orientations. Therefore, the fruit would receive damage in this drop scenario.

Due to horizontal collision with a wooden object, contact force variations in pear assume two rising (loading phase) and falling (unloading phase) trends (Fig. 22). In the loading phase, the maximum contact force was found to be 130.40 N at step 21. Following this step, the loading phase ends and the unloading phase begins that involves reduction in the contact force, where the sample moves opposite the drop direction and loses contact with the surface. A similar phenomenon occurs during vertical collision with the wooden plate, except that the loading phase ends at step 18 and reaching a contact force of 135.08 N (Fig. 22). This behavior in the force plot was in complete agreement with the results obtained by previous researchers [10,37]. During the horizon-

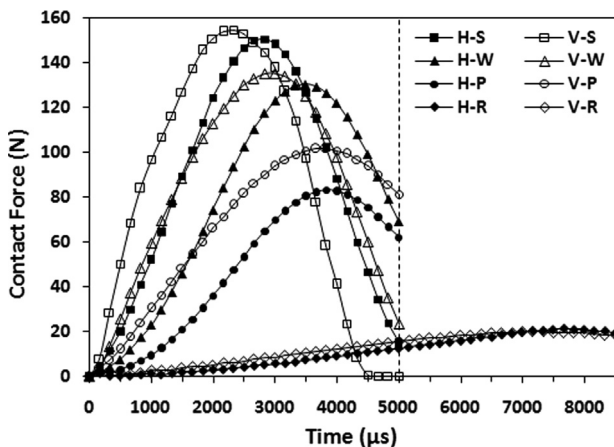


Fig. 22 – Force-time diagram for the collision of pear to rigid and flexible objects: (H) horizontal; (V) vertical; (S) steel; (W) wood; (P) Perspex; (R) rubber.

tal collision of pear with the Perspex surface, the rising trend of the contact force spans from the impact moment to step 23, during which it reaches from 1.61 N to 83.12 N. On the other hand, the unloading process starts following step 23 with a falling trend until reaching a zero contact force (Fig. 22). As observed, during vertical collision with the same surface, there is a rising trend in the loading phase, during which the maximum contact force (101.49 N) occurs at step 22. From this point on, it follows a falling trend. In horizontal collision with the rubber surface, the loading phase extended until 7666 μ s after impact, and then it entered into the unloading phase. In vertical collision of the pear with rubber, the loading phase lasted shorter and ended at 7000 μ s after impact. Following these two thresholds (7666 and 7000 μ s), the rebounding period starts which is the phase during which the contact force gradually decreases until the sample is separated from the surface. Unlike other impact surfaces, the maximum contact force (21.03 N) belonged to the horizontal impact at 7666 μ s after impact. In vertical collision with a non-rigid surface, the highest recorded contact force was 19.86 N (Fig. 22). Regarding this important mechanical parameter, the information from FEM simulations supports the usability of rubber in covering rigid surfaces. This is because the force acting on the fruit produced by collision with a rubber surface is considerably smaller than the force required to reach the failure or biological yield point.

The elastic modulus of the impact material and the radius of curvature of the fruit at the impact location are two major factors determining the damage level. Surfaces with a lower elastic modulus, and thus higher energy absorption capacity, leave less bruises and damages on products [33,39]. Using extended Hertz contact theory, Horsfield et al. [34] reported that a material with a low modulus of elasticity can perform better in reducing the impact-induced bruising in peach fruits, where the material is used to catch the falling fruit. This is in complete agreement with the results of this study, where the largest stresses, strains and contact forces occurred in collision with the steel surface with high Young's modulus. On the contrary, the lowest amount of these

quality-degrading parameters was recorded in collision with the rubber surface that has a very small Young's modulus. This is due to the fact that rubber can act as a cushion and a shield that partly absorbs the impact energy while transferring the rest to the pear [40]. In their experiments, Ahmadi and Abedi [41] and Lewis et al. [33] observed that larger radius of curvature (at the location of impact) caused more damages and bruises. FEM analyses showed that vertical fall leads to larger stresses and strains that can be in relation to the radius of curvature at the impact location.

4. Conclusions

Throughout all engineering majors, it is very important to investigate physical events in a visual manner, particularly to understand and examine material behavior to various dynamic loadings. Under loading conditions, it can be a difficult undertaking to examine this behavior of agricultural materials with their complex structures. In fact, visual investigations give no insight about what happens inside of loaded materials. Computer aided engineering (CAE) applications can be useful in this regard. This study used FEM method to simulate the dynamic behavior of pear fruit when dropped at a height of 207.22 mm on a fixed surface. In the simulation environment, we examined the effects of parameters such as impact surface (i.e. steel, wood, Perspex and rubber) and drop orientation (i.e. vertical and horizontal) on the distribution trends of stresses and strains from the impact moment until reaching their peaks, as well as the maximum magnitude of contact force.

The following points can be concluded according to the research findings:

- The largest stress (0.493 MPa) and strain (0.219) belonged to the vertical collision of the pear with the steel surface, which were developed following 2500 and 2333 μ s after impact, respectively. The minimum stress (0.099 MPa) and strain (0.046) belonged to the horizontal collision of the pear with the rubber surface, which were developed following 7666 and 7333 μ s after impact, respectively.
- Stress and strain peaks were always at the collision location, and their distribution waves generally extended from the impact location towards the pear core.
- The largest (154.41 N) and smallest (19.86 N) contact forces were recorded in vertical collision of pear with the steel and rubber surfaces, respectively.

From the promising results of this study, it is probably safe to infer that FEM modeling can be a cost-effective method for recognizing and examining damages to agricultural products under different loading conditions (harvesting, handling, packaging and storage). It also facilitates the accurate analysis of the results. Future studies should focus on evaluating the effect of drop height on stress, strain and contact force magnitudes, as well as simulating the pear to pear collision mechanism.

REFERENCES

- [1] Dintwa E, Jancsók P, Mebatson HK, Verlinden B, Verboven P, Wang CX, et al. A finite element model for mechanics deformation of single tomato suspension cells. *J Food Eng* 2011;103(3):265–72.
- [2] Miraei Ashtiani SH, Salarikia A, Golzarian MR, Emadi B. Non-destructive estimation of mechanical and chemical properties of persimmons by ultrasonic spectroscopy. *Int J Food Prop* 2016;19(7):1522–34.
- [3] Hashemi Fard Dehkordi SH, Jafarhassani Hanjani P, Chegini GR. Design, construction and evaluation of chrysanthemum flower stem cleaner machine. *Jordan J Mech Ind Eng* 2014;8:369–75.
- [4] Mohammad Shafie M, Rajabipour A, Castro-García S, Jiménez-Jiménez F, Mobli H. Effect of fruit properties on pomegranate bruising. *Int J Food Prop* 2015;18(3):1837–46.
- [5] Miraei Ashtiani SH, Golzarian MR, Baradaran Motie J, Emadi B, Nikoo Jamal N, Mohammadinezhad H. Effect of loading position and storage duration on the textural properties of eggplant. *Int J Food Prop* 2016;19(4):814–25.
- [6] Scherrer-Montero CR, Dos Santos LC, Andreazza CS, Getz BM, Bender RJ. Mechanical damages increase respiratory rates of citrus fruit. *Int J Fruit Sci* 2011;11(3):256–63.
- [7] Opara UL, Pathare PB. Bruise damage measurement and analysis of fresh horticultural products – A review. *Postharvest Biol Technol* 2014;91:9–24.
- [8] Stropek Z, Gołacki K. A new method for measuring impact related bruises in fruits. *Postharvest Biol Technol* 2015;110:131–9.
- [9] Xu R, Takeda F, Kremer G, Li C. Measure of mechanical impacts in commercial blueberry packing lines and potential damage to blueberry fruit. *Postharvest Biol Technol* 2015;110:103–13.
- [10] Celik HK, Rennie AEW, Akinci I. Deformation behaviour simulation of an apple under drop case by finite element method. *J Food Eng* 2011;104(2):293–8.
- [11] Prasertsan S, Peeraprasoppong C, Thamaratwasik P. Impact damage in mangosteens (*Garcinia Mangostana* L.). *Int J Food Prop* 1998;1(3):243–54.
- [12] Komarnicki P, Stopa R, Szyjewicz D, Młotek M. Evaluation of bruise resistance of pears to impact load. *Postharvest Biol Technol* 2016;114:36–44.
- [13] Dintwa E, Van Zeebroeck M, Ramon H, Tijskens E. Finite element analysis of the dynamic collision of apple fruit. *Postharvest Biol Technol* 2008;49:260–76.
- [14] Khodabakhshian R, Emadi B. Development of a finite element method model to determine mechanical behavior of pumpkin seed. *Int J Food Prop* 2015;18(2):231–40.
- [15] Topakci M, Celik HK, Canakci M, Rennie AEW, Akinci I, Karayel D. Deep tillage tool optimization by means of finite element method: case study for a subsoiler tine. *J Food Agric Environ* 2010;8:531–6.
- [16] Kabas O, Vladut V. Determination of drop test behavior of a sample peach using finite element method. *Int J Food Prop* 2015;18(11):2584–92.
- [17] Nowak P. Validation of finite element method solver for utilization in eddy current tomography. In: Jabłoński R, Brezina T, editors. Advanced mechatronics solutions. Springer; 2016. p. 173.
- [18] Kabas O, Celik HK, Ozmerzi A, Akinci I. Drop test simulation of a sample tomato with finite element method. *J Sci Food Agric* 2008;88(9):1537–41.
- [19] Sirisomboon P, Tanaka M, Akinaga T, Kojima T. Evaluation of the textural properties of Japanese pear. *J Texture Stud* 2000;31(6):665–77.
- [20] Wang J. Mechanical properties of pear as a function of location and orientation. *Int J Food Prop* 2004;7(2):155–64.
- [21] Baradaran Motie J, Miraei Ashtiani SH, Abbaspour-Fard MH, Emadi B. Modeling physical properties of lemon fruits for separation and classification. *Int Food Res J* 2014;21:1901–9.
- [22] Lutovska M, Mitrevski V, Pavkov I, Mijakovski V, Radočin M. Mathematical modelling of thin layer drying of pear. *Chem Ind Chem Eng Q* 2016;22:191–9.
- [23] Miraei Ashtiani SH, Emadi B, Sanaei-Moghadam A, Aghkhani MH. Effect of moisture content and temperature on thermal behaviour of sesame seed. *Ann Univ Dunarea Jos Galati Fascicle VI – Food Technol* 2014;38:87–103.
- [24] Aghkhani MH, Miraei Ashtiani SH, Baradaran Motie J, Abbaspour-Fard MH. Physical properties of Christmas lima bean at different moisture content. *Int Agrophys* 2012;26(4):341–6.
- [25] ASABE Standards. Compression test of food materials of convex shape S368.4. American Society of Agricultural and Biological Engineers; 2008.
- [26] Kim GW, Do GS, Bae Y, Sagara Y. Analysis of mechanical properties of whole apple using finite element method based on three-dimensional real geometry. *Food Sci Technol Res* 2008;14:329–36.
- [27] Bentini M, Caprara C, Martelli R. Physico-mechanical properties of potato tubers during cold storage. *Biosyst Eng* 2009;104(1):25–32.
- [28] Al-Qadi IL, Wang H, Tutumluer E. Dynamic analysis of thin asphalt pavements by using cross-anisotropic stress-dependent properties for granular layer. *Transp Res Rec* 2010;2154:156–63.
- [29] Tsang-Mui-Chung M, Verma LR, Wright ME. A device for friction measurement of grains. *Trans ASAE* 1984;27(6):1938–41.
- [30] Chung JH, Verma LR. Determination of friction coefficients of beans and peanuts. *Trans ASAE* 1989;32(2):745–50.
- [31] Kabas O, Vladut V. Determination of some engineering properties of pecan (*Carya illinoiensis*) for new design of cracking system. *Erwerbs-Obstbau* 2016;58(1):31–9.
- [32] Celik HK, Karayel D, Caglayan N, Rennie AEW, Akinci I. Rapid prototyping and flow simulation applications in design of agricultural irrigation equipment: case study for a sample inline drip emitter. *Virtual Phys Prototyp* 2011;6(1):47–56.
- [33] Lewis R, Yoxall A, Canty LA, Reina Romo E. Development of engineering design tools to help reduce apple bruising. *J Food Eng* 2007;83(3):356–65.
- [34] Horsfield BC, Fridley RB, Claypool LL. Application of theory of elasticity to the design of fruit harvesting and handling equipment for minimum bruising. *Trans ASAE* 1972;15(4):746–50.
- [35] Seyedabadi E, Khojastehpour M, Sadrnia H. Prediction cantaloupe bruising using non-linear finite element method. *Int J Food Prop* 2015;18(9):2015–25.
- [36] Sun C, Wang L, Wang Z, Geng L, Li D, Sui M, et al. Finite element analysis of a retrieved custom-made knee prosthesis. *J Mech Med Biol* 2015;15:1550020–34.
- [37] Ahmadi E, Barikloo H, Kashfi M. Viscoelastic finite element analysis of the dynamic behavior of apple under impact loading with regard to its different layers. *Comput Electron Agric* 2016;121:1–11.
- [38] Herold B, Geyer M, Studman CJ. Fruit contact pressure distributions-equipment. *Comput Electron Agric* 2001;32:167–79.
- [39] Zhou J, He L, Karkee M, Zhang Q. Effect of catching surface and tilt angle on bruise damage of sweet cherry due to mechanical impact. *Comput Electron Agric* 2016;121:282–9.
- [40] Jarimopas B, Singh SP, Sayasoothorn S, Singh J. Comparison of package cushioning materials to protect post-harvest impact damage to apples. *Packag Technol Sci* 2007;20:315–24.
- [41] Ahmadi E, Abedi G. Sensitivity of tomatoes to internal bruising induced by mechanical stress. *Europ J Hort Sci* 2013;78(5):219–24.